Science of the Total Environment xxx (xxxx) xxx

Contents lists available at ScienceDirect

Science of the Total Environment

journal homepage: www.elsevier.com/locate/scitotenv

Field test of the surface soil moisture mapping using Sentinel-1 radar data

A.M. Zeyliger [a,*], K.V. Muzalevskiy [b], E.V. Zinchenko [c], O.S. Ermolaeva [a]

[a] Russian State Agrarian University – Moscow Timiryazev Academy, Moscow, Russian Federation
[b] Kirensky Institute of Physics of the Siberian Branch of the RAS – Division of Federal Research Center, Krasnoyarsk Scientific Center of the Siberian Branch of the RAS, Krasnoyarsk, Russian Federation, Siberian Federal University, Krasnoyarsk, Russian Federation
[c] All-Russian Scientific Research Institute of Irrigated Agriculture, Volgograd, Russian Federation

HIGHLIGHTS

- Formation of soil water erosion and preferential water flow during irrigation negatively impacted surface and ground water bodies.
- Mapping of soil water moisture (SWM) by Remote Sensing for precision irrigation is motivated.
- A model to map SWM of soil surface using Sentinel-1 radar data is developed.
- Test field confirms a satisfactory linear correlation between in situ measured and in vitro calculated SWMs.
- Developed model can be used to map SWM by radar for the purpose precision irrigated management.

GRAPHICAL ABSTRACT

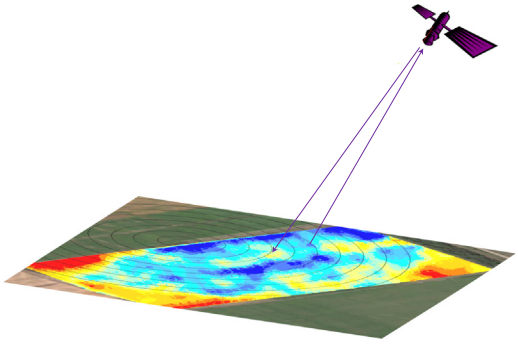

ARTICLE INFO

Article history:
Received 15 January 2021
Received in revised form 13 October 2021
Accepted 17 October 2021
Available online xxxx

Guest Editor: Leonor Rodriguez-Sinobas

Keywords:
Sentinel-1
UAV
Digital elevation model
Radar backscattering
Artificial neural network
Soil moisture

ABSTRACT

Soil surface moisture is one of the key parameters for describing the hydrological state and assessing the potential availability of water for irrigated plants. Because the radar backscattering coefficient is sensitive to soil moisture, the application of Sentinel-1 data may support soil surface moisture mapping at high spatial resolution by detecting spatial and temporal changes at the field scale for precision irrigation management. This mapping is required to control soil water erosion and preferential water flow to improve irrigation water efficiency and minimise negative impacts on surface and ground water bodies.

Direct observations of soil surface moisture (5-cm thickness) were performed at an experimental plot in the study site of the All-Russian Scientific Research Institute of Irrigated Agriculture, near the village Vodnyy, Volgograd region. Soil surface moisture retrieval from Sentinel-1 was performed at the same location. A second set of soil surface moisture was calculated for the soil sampling sites using the permittivity model, based on the estimates of soil surface characteristics: a) reflectivity, obtained by the neural network method from Sentinel-1 observations; b) roughness, obtained from the geodata of the stereoscopic survey with unmanned aerial vehicle Phantom 4 Pro.

The raster set of soil surface moisture geodata was obtained based on the reflectivity geodata raster set to solve the inverse problem using a permittivity model that considers the soil texture of the experimental plot. The determination coefficient (0.948) and standard deviation (2.04%) were obtained by comparing both sets of soil moisture point geodata taken from the same soil sampling sites. The values confirmed a satisfactory linear correlation between the directly measured and indirectly modelled sets. A comparison of the two sets of geodata indicated a satisfactory reproduction of the first set by the second set.

* Corresponding author.
E-mail addresses: azeiliguer@mail.ru, azeyliger@gmail.com (A.M. Zeyliger), rsdkm@ksc.krasn.ru (K.V. Muzalevskiy), zinchenko_ev@vniioz.ru (E.V. Zinchenko).

https://doi.org/10.1016/j.scitotenv.2021.151121

Please cite this article as: A.M. Zeyliger, K.V. Muzalevskiy, E.V. Zinchenko, et al., Field test of the surface soil moisture mapping using Sentinel-1 radar data, Science of the Total Environment, https://doi.org/10.1016/j.scitotenv.2021.151121

As a result, the developed method can be considered as the scientific and methodological basis of the new technology of soil surface moisture monitoring by radar, which is one of the basic characteristics used in precision irrigation management.

1. Introduction

For global, regional, and local hydrological dynamic modelling of water storage at the soil cover and its root zone, the soil moisture of the soil surface layer (SSL) Θ_{ss} is one of the key dynamic characteristics. Information derived from various aerospace and ground monitoring systems is used to remotely assess Θ_{ss}^{rs} (superscript "*rs*" means remote sensing) at different spatial and temporal resolutions during natural meteorological conditions and during periods of agricultural crop irrigation (Andreassian et al., 2006; Chen et al., 2005; Gowda et al., 2008; Moehrlen, 1999; Muzylev et al., 2017; Overgaard et al., 2006; Pitman, 2003; Startseva et al., 2014).

At the same time, Θ_{ss}^{rs} may be used to control soil water erosion and preferential water flow during crop irrigation in chernozem soil (Khitrov et al., 2009; Zatinatskii et al., 2007), which is necessary to optimise irrigation water use efficiency (Zeyliger et al., 2019) and protect the environment against the negative impact of irrigation (Khitrov et al., 2009; Zatinatskii et al., 2007). One of the technologies that addresses the temporal and spatial variability of soil moisture within a field is called precision irrigation or variable-rate irrigation. This technology is used to deliver the desired amount of water to specific locations in an irrigated area (Evans et al., 2015). Many studies have been conducted on the use of point-scale sensors installed in the field to gather information on soil moisture content (Dukes and Scholberg, 2004; Evett and Parkin, 2005; Robinson et al., 2008, Vellidis et al., 2007, Sui and Baggard, 2015). However, their implementation at the field scale requires a dense monitoring network that is resource consuming. Few studies have focused on the development of methods for mapping soil moisture from space. Thus, this study aimed to develop a remote sensing method for soil surface moisture to control zones with risk of soil water erosion, and the development of preferential water flow.

Sentinel-1 radar enables new approaches for the space monitoring of Θ_{ss}^{rs}. Unlike the sensors operating in the infrared spectrum, the microwave radiation of Sentinel-1 operates at a C-range of frequencies (5.4 GHz) and does not depend on light conditions and unfavourable atmospheric phenomena, allowing 24-h and all-weather monitoring. In contrast to the modern satellite radiometers of SMAP and SMOS/MIRAS (L-band, *1.4 GHz*) (Entekhabi et al., 2014; Wigneron et al., 2017), GCOM-W1/AMSR2 (K- and Ku- bands, *19* and *37 GHz*, respectively) (Gao et al., 2018), as well as the Metop/ASCAT radar (C-band, *5.3 GHz*) (Brocca et al., 2017), which have a low spatial resolution of *~10 km*, the Sentinel-1 radar has a spatial resolution *of ~10 m*. The high spatial resolution of the Sentinel-1 radar enables new approaches to distinguish even small and narrow parcels of non-homogeneous land within the irrigated field for space monitoring of Θ_{ss}^{rs}.

In general, in territories occupied by agricultural crops, the key characteristics affecting the backscatter coefficient, which is measured by the Sentinel-1 radar at a fixed angle (*29–46°*), are soil moisture and soil surface roughness (Oh et al., 1992). In particular, when the soil surface is devoid of vegetation, the key characteristics are Θ_{ss} and roughness of daylight SSL. These characteristics change in time and space, and the rate of these changes is closely related to the characteristics of meso- and macro-relief, as well as the characteristics of the soil and vegetation surface layer. The drivers of such changes have various natural and anthropogenic impacts on the soil surface and vegetation layer. For agricultural lands, such drivers are phenomena that provoke water and wind erosion, as well as agricultural cultivation of land and irrigation of crops, which in some cases provokes irrigation erosion.

The use of statistical characteristics of the soil surface roughness h_{ss} is one method to represent the soil roughness in existing scattering models. In widely used models, such as the small perturbation method, physical and geometric optics, semi-empirical models, and integral equation method (Ulaby and Long, 2014), the input parameters are Θ_{ss}, the standard deviation $\sigma(h_{ss})$, correlation length, and autocorrelation function $F(h_{ss})$ of the surface elevation. In addition, $\sigma(h_{ss})$, the correlation length, and the type of $F(h_{ss})$ measured in agricultural fields depend on the profile length (*0.5–25 m*) of acquisition (Davidson et al., 2000). As a result, the model estimates of Θ_{ss}^{rs} from satellite radar data based on existing classical scattering models using the statistical parameters of the roughness of SSL lead to large discrepancies with the field measurement data (Wang et al., 2014; Baghdadi et al., 2004, 2011; Thoma et al., 2006). In recent years, semi-empirical approaches based on the use of neural network (NN) methods have been widely used to overcome these limitations. Baghdadi et al. (Baghdadi et al., 2004) proposed a modified integral equation-based scattering model, in which one of the input parameters (correlation length) was calibrated with respect to the measured values of $\sigma(h_{ss})$ at the test sites. By applying this approach, the authors were able to reduce the error of the posterior estimate of the backscatter coefficient up to *0.9–2.2* times. Moreover, in such scattering models, the topsoil permittivity is used as an input parameter, which is calculated using empirical and physical-based permittivity models (Dobson et al., 1985; Hallikainen et al., 1985; Mironov et al., 2009; Zhang et al., 2020). The empirical model (Hallikainen et al., 1985) uses Θ_{ss} and soil texture f_d as input parameters. In addition to these input parameters (Hallikainen et al., 1985), the semi-empirical model (Dobson et al., 1985) also uses the soil characteristics, such as dry bulk density, density of the soil solid phase, and frequency of the electromagnetic wave as input parameters. Among the known dielectric models in the microwave band, the best results are provided (Mialon et al., 2015) by the physical model (Mironov et al., 2009), which is currently used in the SMOS (Wigneron et al., 2017) and SMAP (Zeng et al., 2016) algorithms for global monitoring of the SSL moisture. This model allows the calculation of the complex permittivity of soils with a clay fraction f_{clay} (soil elementary particle size *<0.002 mm* according to the United States Department of Agriculture classification) depending on volumetric moisture Θ_{ss} and wave frequency in the range of *45 MHz–26.5 GHz* at temperatures of *20–22*°C. This model was validated on a dataset of *15* soil types, with a clay content *of 0–76%*.

In recent years, considerable progress in the development of semi-empirical approaches has been achieved by the combination of integral equation physical-based scattering models with artificial intelligent methods, which are used to calculate Θ_{ss}^{rs} using the values of the backscatter coefficient (Mirsoleimani et al., 2019). The use of Sentinel-1 radar data on vertical-vertical (VV) polarization and neural networks (NNs) with two hidden layers and *20* neurons enabled the estimation of the backscatter coefficient with an accuracy of *0.8 dB,* and consequently, the calculation of Θ_{ss}^{rs} of bare soil with accuracy in the order of *0.03* m^3m^{-3} (Mirsoleimani et al., 2019). In the case of canopy soil, with a maximum normalized difference vegetation index (NDVI) of *0.75* and $\sigma(h_{ss})$ within *1–3 cm*, the accuracy of the posterior estimate of Θ_{ss}^{rs} increases to *0.05* m^3m^{-3} using a single VV polarization, or a pair of VV and vertical-horizontal (VH) polarizations (El Hajj et al., 2017). Similar results were obtained in a previous study (El Hajj et al., 2016) for an X-band radar using both a single horizontal-horizontal (HH)

polarization and a pair of HH-VV polarisations. The corresponding algorithms for solving inverse problems in cases of large volumes of radar data when combining semi-empirical methods and NNs for monitoring purposes of Θ_{ss}^{rs} are considerably complex. However, the achieved positive results indicate significant prospects for this methodology. Paloscia et al. (2008) proposed an efficient algorithm for posterior estimation of Θ_{ss}^{rs} based on the feed-forward NN, utilizing the radar data (HH and HV polarisations) of the ENVISAT/ASAR satellite in the C-band for several test fields in northern Italy. They obtained a standard deviation of *2.2–2.8%* and a determination coefficient of $r^2 = 0.85–0.91$ relative to the invasive measurement dataset of Θ_{ss}^{gr} (superscript "gr" means ground). A similar approach using Sentinel-1 radar data, Radarsat, and Envisat was applied to the test plot located on agricultural lands in Italy, Australia, and Spain (Paloscia et al., 2013), as well as Tunisia (Hachani et al., 2019). As a result, the deviations of a posteriori estimates of the radar data of Θ_{ss}^{rs} from ground measuring data of Θ_{ss}^{gr} were in the range of *0.02–0.05* m^3m^{-3}. An analysis of the literature also indicated that during the soil moisture retrieval, the use of any pair of polarisations (HH and HV, VV, and VH) as input parameters of the NN enables to consider the soil surface roughness for bare soils or soils rarely covered by vegetation.

In contrast to existing approaches (El Hajj et al., 2017; Mirsoleimani et al., 2019, El Hajj et al., 2016; Paloscia et al., 2008, Paloscia et al., 2013; Hachani et al., 2019), we use a neural network to estimate the reflectivity of the soil, not directly the soil moisture. This approach makes it possible to take into account the content of the clay fraction in the SSL based on the use of a dielectric model. In order to study in detail, the effect of soil surface roughness and topography on the spatial distribution of Θ_{ss}, a high-resolution digital elevation model (DEM) was used. This DEM was produced from Unmanned Aerial Vehicle (UAV) data set performed synchronously with the polarimetric Sentinel-1 observations.

2. Materials and methods

2.1. Experimental site and soil specification

The studies for testing the developed method of a posteriori estimation of Θ_{ss} were conducted on the territory of the experimental agricultural production farm of the All-Russian Scientific Research Institute of Irrigated Agriculture (VNIIOZ), near the village Vodnyy, Volgograd region (see Fig. 1). Climate of territory is classified as moderately continental, with moderately cold winters and hot summers. The soil type at this territory is Luvic Kastanozem (IUSS Working Group WRB, 2015). It is middle loamy in texture and has the typical characteristics of such soils in Volgograd region of Russia.

The coordinates of the centre of the experimental plot (48.60367°N, 44.15659°E) correspond to the intersection of lines A-B and A1-B1 (see Fig. 1), where they are displayed on top of the NDVI map derived from the red and near infrared (NIR) data Sentinel-2 on 21st August 2019. The plot with area about 3 ha is located on a relatively flat transverse slope, with a slope in the direction from north to south (along line A-B) of approximately *2%*. The ground truth of Θ_{ss}^{gr} monitoring was

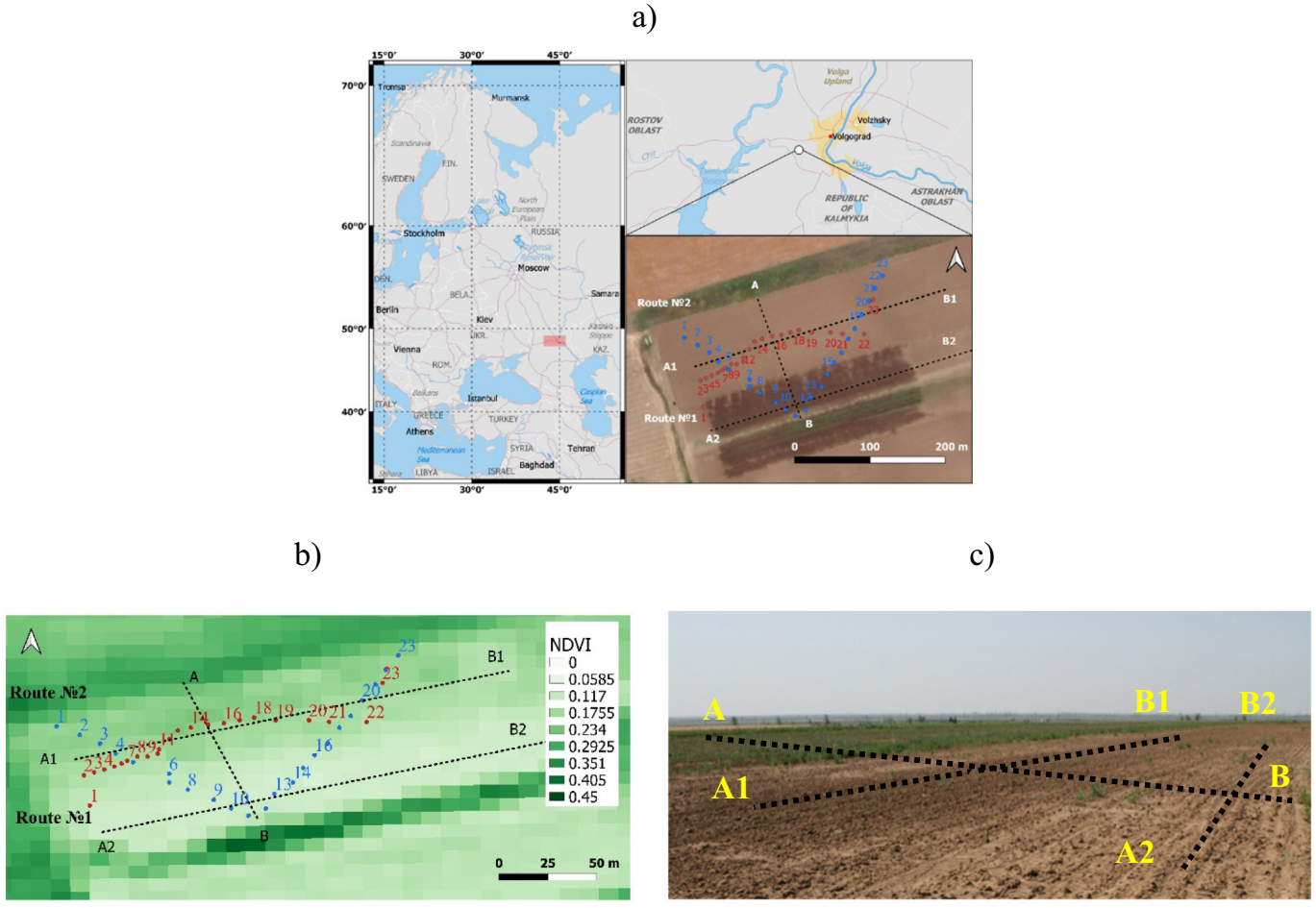

Fig. 1. The experimental plot located on the fields of VNIIOZ: a) Global map; b) NDVI maps calculated from Sentinel-2 space image in Red and Near Infrared channels (red for Route № 1 and blue for Route № 2 dots indicate places of soil sampling); c) ground image of the experimental plot. (For interpretation of the references to colour in this figure legend, the reader is referred to the web version of this article.)

conducted at the time of the Sentinel-1 flight (20th August 2019). One part of the experimental plot, located between its middle and northern borders, was partially covered by rare alfalfa. The second part, located between the middle and southern borders, was bare soil (see Fig. 1 c). The soil surface at the experimental plot had a rather pronounced microrelief, which was formed as a result of the ploughing of irrigated alfalfa crops across the slope shortly before the Sentinel-1 flight. The difference between the bare soil plots and those covered by alfalfa residues was confirmed by the NDVI values, calculated according to the Sentinel-2 constellation data (Fig. 1 b). Therefore, for the northern and southern parts of the experimental plot, the NDVI values appeared to be 0.103 ± 0.007 and 0.176 ± 0.022, respectively.

2.2. Experimental methodology and ground truth measurements

The experimental methodology consisted of two parts. The first part (ground) was focused on obtaining a set of instantaneous georeferenced data of Θ_{ss}^{gr}, as well as daytime surface characteristics such as elevation, soil texture, and roughness at the sampling point scale. The second part (computer) was focused on the development of the algorithm, debugging, and testing of tools for processing the basic data of ground monitoring and radar surveys, including the final calculation of the posterior estimate of the Θ_{ss}^{rs} at the radar pixel scale obtained by remote sensing data and its comparison with Θ_{ss}^{gr} obtained at the point scale. The ground field part of the experimental work consisted of obtaining datasets of elevation characteristics and Θ_{ss}^{gr} selection for two monitoring routes No. 1 and No. 2 (Fig. 1). The first of route started at the southern boundary of the experimental plot. It moved along the oblique line to the northern boundary, after which it changed direction to the southern boundary of the experimental plot. The second route was a mirror image of the first, and accordingly, it started and ended on the northern border of this plot. The spatial configuration of the monitoring routes was planned and implemented to optimally cover the field monitoring of various elements of the SSL in the experimental plot.

Sampling sites along the routes were selected based on visual analysis of the soil surface meso-relief such that they were in the centre of the representative plots of 1–2 m size. For the convenience of digital recording, as well as subsequent interpretation of field monitoring results, a special mobile application was developed in the ArcGIS Online software environment with a set of necessary tabs and tools for collecting primary data and transmitting it via mobile communication to the database in the specified cloud geo-service. The main data collected were: a) date and time of soil sampling; b) coordinates of soil sampling sites; c) numbers of soil sampling rings; g) videos of soil sampling sites and relevant soil sampling rings identified by numbers. This procedure significantly simplified the field monitoring and processing of laboratory measurements, as well as the final cartographic interpretation of the results. In general, the developed field monitoring procedure allowed the automation of the process of filling in the layers of the geodata database, as well as to conduct soil sampling at planned plots, using a template prepared in advance.

The selection of undisturbed soil samples was performed with a sampler and soil sampling rings of height *5 cm* with a cutting edge produced by the Dutch company Eijkelkamp. Using this sampler, the rings were vertically deepened in SSL. When the top of the ring was at the soil surface level, it was pulled out together with the soil sample, which filled its internal volume, and its two open faces were hermetically closed with regular soft plastic covers. The bulk density and soil moisture of the obtained samples were subsequently determined in the soil laboratory of VNIIOZ using the standard gravimetric method. Θ_{ss}^{gr} SSL datasets were obtained by the ground monitoring performed on 20 August 2019 at the experimental plot of the experimental production farm of VNIIOZ (approximately *2 ha*) using the method described above, at 46 points for both routes No.1 and No.2 (Fig. 1).

2.3. Space and airborne observations

Stereoscopic image recording of the experimental plot was performed using the Dji Phantom 4 Pro UAV, equipped with a camera to assess the elevation characteristics along both monitoring routes. As a result of processing the received digital image data in the Agisoft PhotoScan v. 1.3.0 (GeoScan, Russia) *photogrammetry* software, a digital elevation model (DEM) was created, tied to georeferenced centres of the dots with a sub-centimetre resolution and corresponding differentiated corrections.

For the territory of the experimental plot, the complex values of the backscatter coefficient (σ_{VV}, σ_{VH}) at VV and VH polarizations were measured on 20th August 2019 by Sentinel-1A at a frequency of *5.4 GHz* in the interferometric broadband mode (IW SLC images projected on Earth's surface using the Earth ellipsoid model) with a spatial resolution of ~10 m. The data in the standard format (Standard Archive Format for Europe, SAFE) were obtained from the European Space Agency Data Centre (Copernicus Open Access Hub, 2020) and processed with ESA SNAP v.7 (European Union) software. Due to the different spatial resolution for different datasets, the backscattering coefficient measured by Sentinel-1 were interpolated (based on origin 2D grid) to obtain the backscattering coefficients at the coordinate exactly corresponding to the soil moisture sampling point. In order to study the features of the scattering properties of the soil's surface of the experimental plot, the polarimetric analysis was carried out on the basis of the H-α-decomposition for two polarizations VV and VH in accordance with the work (Cloude, 2007).

3. Method of a posteriori estimation of surface soil moisture based on Sentinel-1 geodata using a neural network

The developed method of a posteriori estimation of Θ_{ss}^{rs} from remote sensing data is based on the use of a NN method. In this work, we chose the simplest feed-forward NN, consisting of 1–4 hidden layers with 1–30 neurons each. NN modelling was performed using the MATLAB software environment. Reflectivity in nadir observation, $\Gamma_0(\Theta ss, f_{\text{clay}})$, where f_{clay} is the clay content, was used as the output value, and the backscatter coefficients (σ_{VV},σ_{VH}) were used as input values for the NN. For the NN, 32 training pairs of input values (σ_{VV},σ_{VH}) and 32 $\Gamma_0(\Theta_{ss}, f_{clay})$ values were used. Input and output values were randomly chosen from the 46 values of the σ_{VV},σ_{VH}, $\Gamma_0(\Theta_{ss}, f_{clay})$ set, in correspondence with the soil sampling locations (Fig. 1). The $\Gamma_0(\Theta_{ss}, f_{clay})$ values were calculated by the Fresnel equation using the permittivity model (Mironov et al., 2009) (with the clay content of $f_{clay} = 35\%$) and Θ_{ss}^{gr} pedologic dataset measured by the gravimetric method at the sampling sites (Fig. 1a). During training of the NN, the standard Levenberg-Marquardt algorithm was used to minimise the standard deviations between the Γ_0^N output values calculated by the NN and the $\Gamma_0(\Theta_{ss}^{gr}, f_{clay})$ values calculated using *the* Θ_{ss}^{gr} soil dataset. Finally, the predicted Θ_{ss}^{rs} was calculated by solving the inverse problem of minimising the residual norm between the Γ_0^N values predicted by the NN and the $\Gamma_0(\Theta_{ss}^{rs}, f_{clay})$ values calculated based on the Fresnel equation and the dielectric model (Mironov et al., 2009). This minimisation problem was also solved using the Levenberg-Marquardt algorithm. The proposed method of a posteriori estimation of surface soil moisture is schematically depicted in Fig. 2.

General testing of the NN and the method of a posteriori estimation of Θ_{ss}^{rs} according to the scheme presented in Fig. 2 showed that an increasing number of used neurons from 1 to 12 in each of the hidden layers led to an increase in the determination coefficient and a decrease in the standard deviation ($\Delta\Theta_{ss}^{rs}$) between the estimated Θ_{ss}^{rs} and measured values Θ_{ss}^{gr} (Fig. 3). However, using

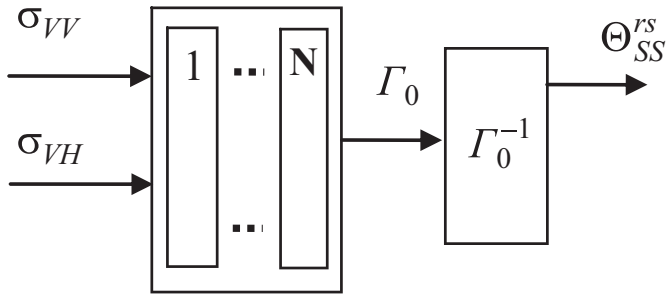

Fig. 2. Simple feed-forward neural network with *N* hidden layers.

two or more hidden layers does not increase the accuracy of the NN estimates.

Computer testing of the NN for various pairs of input data combinations, $q = \sigma_{VH}/\sigma_{VV}, \sigma_{VV}, \sigma_{VH}, \sigma_{VV}$, and σ_{VH}, indicted that the highest value of the determination coefficient between Γ_0^N and $\Gamma_0(\Theta_{ss}^{gr}, f_{clay})$ was obtained for the combination of σ_{VV} and σ_{VH}. As a result, for working purposes, we selected the NN consisting of two hidden layers of 12 neurons each, which allowed us to estimate the Θ_{ss}^{rs} values for all 46 soil sampling sites in the experimental plot with a determination coefficient of $R^2 = 0.948$ and $\Delta\Theta_{ss}^{rs} = 2.04\%$ (see Fig. 4).

In general, the measured Θ_{ss}^{gr} and predicted Θ_{ss}^{rs} data sets of both routes presented in two diagrams in Fig. 5 form two similar correlation functions. This similarity lies in a fairly clear linear correspondence of the analyzed data sets in the range of values exceeding 12% and somewhat less clear in the range with less than this value.

4. Discussion and analysis of the results

According to the DEM data, the h_{ss} profiles of the elevation of the daylight SSL were constructed (see Fig. 5), corresponding to the three lines A-B, A1-B1, and A2-B2, as shown in Fig. 1. Along the monitoring routes, $\sigma(h_{ss})$ of the daylight SSL was calculated (Fig. 5) on square plots of the soil surface, whose centres coincided with the points of soil sampling (Fig. 1).

The middle part of route No. 2, as shown in Fig. 5 a had a lower surface elevation and statistically rougher surface in relation to the central part of route No. 1 (Fig. 5 b). In addition, at the beginning and at the end of route No. 2 there are areas with upper surface elevation and high values of $\sigma(h_{ss})$. An analysis of the locations of the measured and predicted values situated in the noted above middle part of route No. 2 shows that values match the zone with fairly clear linear correspondence (Fig. 6 a).

Continuing the analysis, it should be noted that on graph 6a, site points from 6 to 17 of the route No. 2, lying in its middle part, form a zone with a negative angle of inclination to the axis of surface elevation.

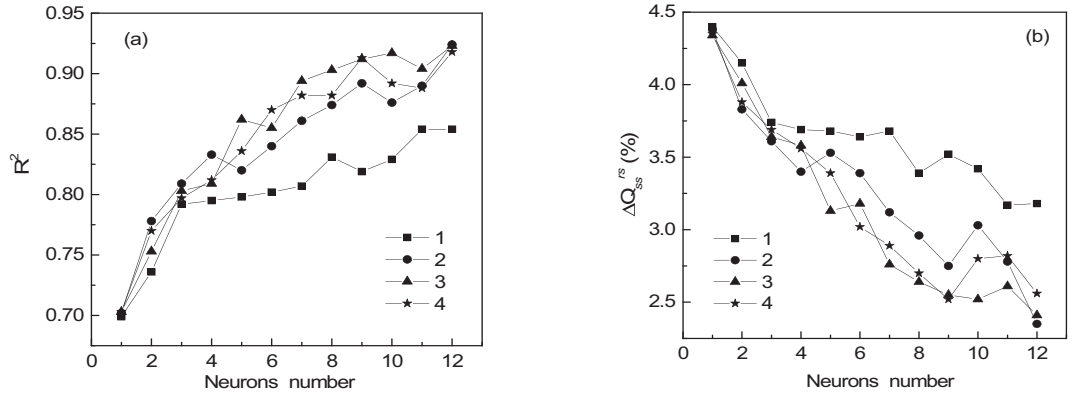

Fig. 3. Accuracy of neural network estimates with number of neurons from 1 to 4 hidden layers: a) determination coefficient between Γ_0^N and $\Gamma_0(\Theta_{ss}^{gr}, f_{clay})$; b) standard deviation between Θ_{ss}^{rs} and Θ_{ss}^{gr}.

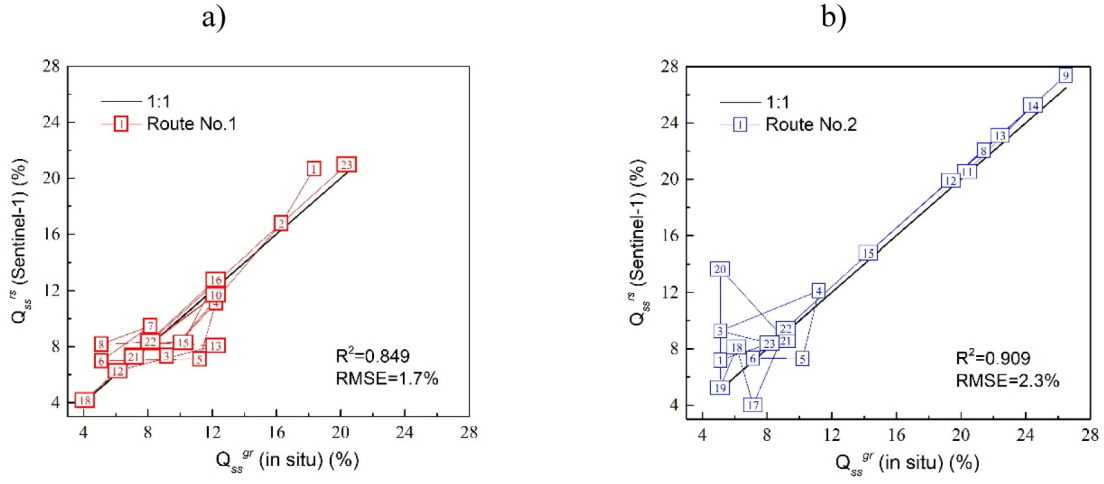

Fig. 4. Comparison between measured in situ Θ_{ss}^{gr} surface soil moisture values and predicted Θ_{ss}^{rs} from remotely sensed data values: a) along routes No. 1 and No. 2; b) along routes No. 2. RMSE: root-mean-square deviation.

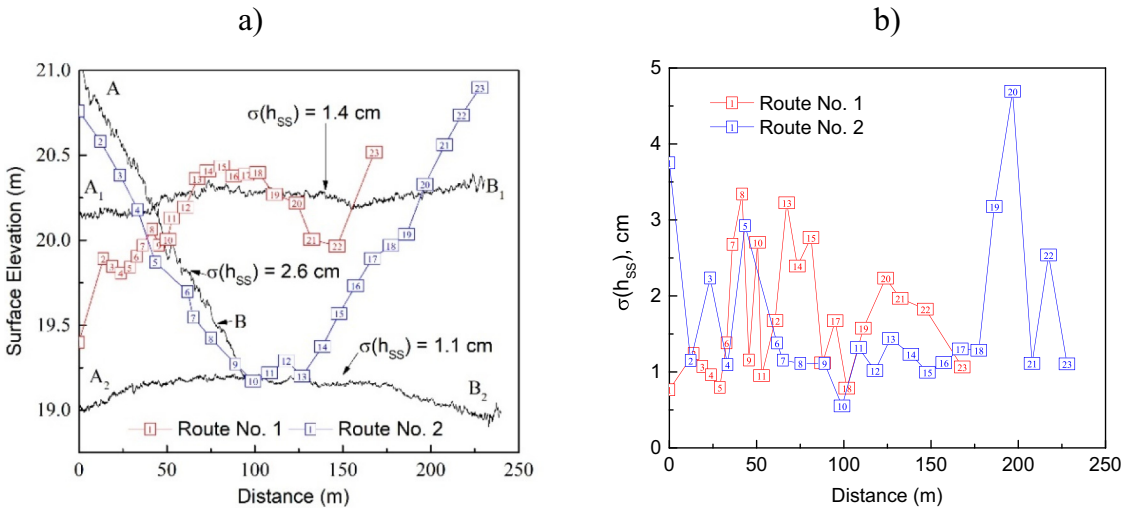

Fig. 5. Parameters of daylight soil surface along routes No. 1 and No. 2: a) surface elevation; b) roughness standard deviation $\sigma(h_{ss})$.

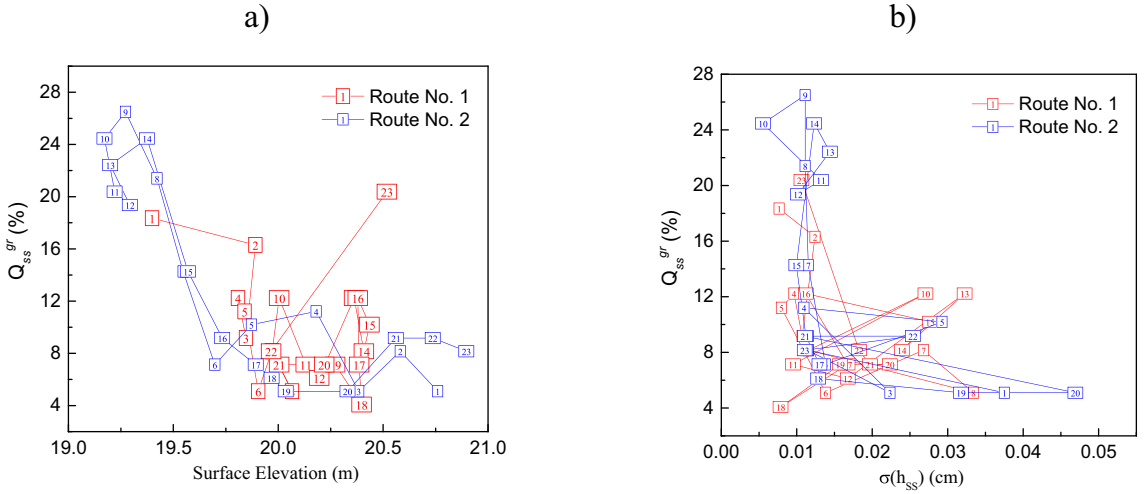

Fig. 6. Measured in situ Θ_{ss}^{gr} profiles along routes No.1 and No.2 on 20th August 2019 as a function of: a) surface elevation; b) roughness standard deviation $\sigma(h_{ss})$.

Apparently, this is the result of the location of these points in the saucer-shaped *meso* depression that was shortly flooded due to irrigation done before soil sampling. Obviously, in this flooded meso depression there was a gradual decrease of level of water stored in it. This led to the formation of the sequence of the appearance of daylight SSL from under the water. And at the time of soil sampling, there was a recorded differentiation of the soil moisture of SSL marked by surface level values.

The conducted polarimetric analysis based on H-α decomposition using complex images of the experimental plot on VH and VV polarizations revealed single-scattering mechanism by the rough soil surface between site points noted above 6 and 17 of the route No. 2 inclusive. As it is noted above these points correspond to the location of the saucer-shaped meso depression, and by the starting and ending points of the route No. 2 (Fig. 7, zones Z9 and Z6 with an entropy value of ~*0.5*). The results of this analysis agree with the statistically high values of the soil surface roughness of the corresponding plots on both routes, as well as the image of the experimental plot (Fig. 1). In addition, the surface layer of the saucer-shaped meso-depression is formed by thin soil particles deposited there from the corresponding watershed areas as a result of surface runoff of not infiltrated rain and irrigation water.

Other locations of soil sampling sites are characterised by high values of α angle and entropy, which indicate predominantly single with diffuse-scattering mechanisms due to the random influence of soil surface and vegetation cover. Additional scattering influence (see

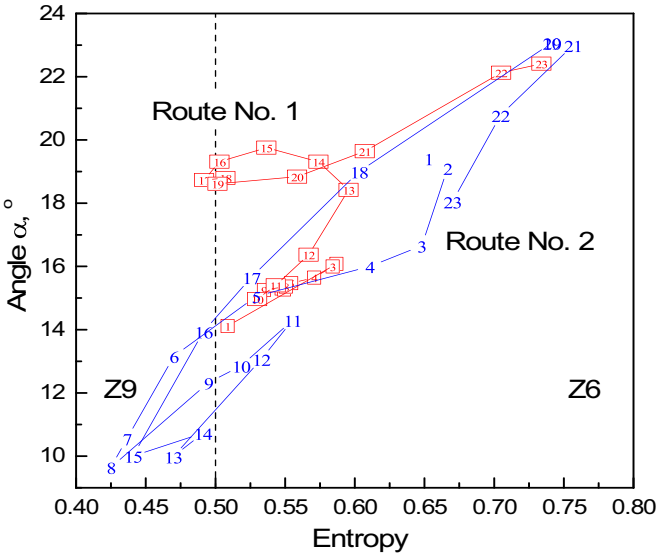

Fig. 7. Characteristics of the experimental plot based on H-α decomposition.

Fig. 7, entropy *>0.5*) of vegetation cover is observed at almost all points of the route No. 1, and endpoints of the route No. 2, which are mainly located in the northern parts of the field that was not ploughed. In addition, it can be noted that the greatest error of a posteriori estimation of Θ_{ss}^{rs} by NN (Fig. 7) is observed for those points along the routes, which are mainly located higher than the average level of soil surface roughness (Fig. 2), as well as those located in zone Z6 (Fig. 7).

Analysis of the data presented in Fig. 7 shows that within the range of *4–13%* of the Θ_{ss}^{gr} values (where the greatest variance is observed), there are statistically more points located in those regions of the route, where soil roughness is increased (*2–4 cm*) (Fig. 5). High Θ_{ss}^{rs} values of *>14%* were typical for the soil sampling points, which were located in the regions of the route with an average level of soil roughness (*< 1.5 cm*). This analysis allows us to conclude that in the areas characterised by medium roughness and high Θ_{ss}^{gr} values, the NN allows for a high degree of confidence to describe the statistical properties of soil surface roughness, as well as the dependence of the backscatter coefficient on Θ_{ss}^{gr}. In the case of small Θ_{ss}^{gr} values of <14% and high values of soil surface roughness, an additional parameter is required. Such additional parameters would independently characterise the $\sigma(h_{ss})$ statistical properties of soil roughness to reduce the variance of the Θ_{ss}^{rs} values estimated in this area. This parameter can be $\sigma(h_{ss})$ values, estimated at the experimental plot by the UAV on the day when Sentinel-1 passes.

The optimal version of the NN obtained during computer testing was used to estimate Θ_{ss}^{rs} over the entire area of the experimental plot (Fig. 8. The cartogram of a posteriori estimation of Θ_{ss}^{rs} presented in this figure generally corresponds to the spatial distribution of Θ_{ss}^{gr} at soil sampling sites during ground truth monitoring. In particular, this is clearly seen from the synchronous differences in the values of both Θ_{ss} pedologic datasets in the meso-relief lowering and *meso*-relief water collection areas at the crossing of the profile lines A-B and A1-B1.

Planning of ground monitoring routes was aimed at obtaining Θ_{ss}^{gr} ground data in a relatively homogeneous area in places with different characteristics of soil surface roughness.

As a result of field monitoring, a pedologic dataset was obtained. One part included information about the area of the saucer-shaped closed meso-relief lowering, and the other part included information about its water collection area. The Θ_{ss}^{gr} values for lowering the meso-relief were expected to be slightly higher than the corresponding values in the water collection area due to the earlier spray irrigation by the sprinkler machine. In general, this assumption is reflected in the results of monitoring, which are presented as Θ_{ss}^{gr} profiles in Fig. 6, where the numbers of soil sampling sites along both routes No. 1 and No. 2 are the values of the abscissa axis.

By visual analysis of the moisture profiles for the routes No. 1 and No. 2 represented in Fig. 6, it is observed the relative similarity of corresponding Θ_{ss}^{gr} values at the beginning and end, as well as a significant difference in these values in the middle parts of both routes. This difference can be explained by the fact that the middle part of the route No. 2 passes through the above-mentioned meso-relief lowering, whereas a result of surface runoff caused by the sprinkling irrigation led to the water storing at meso depression.

The analysis of the results represented in Figs. 4 and 8 shows good comparability of Θ_{ss}^{gr} and Θ_{ss}^{rs} data in the areas where their values are high (which is the saucer-shaped closed meso-depression for route No. 2). This comparability was slightly worse for the relatively drier SSL at the slop of watershed. These differences can be explained by the higher uniformity of the SSL at low sites and a higher degree of heterogeneity in watershed areas.

5. Conclusion

This is the first study focused on the possible use of an NN for processing Sentinel-1 radar data for the purpose of spatial monitoring of

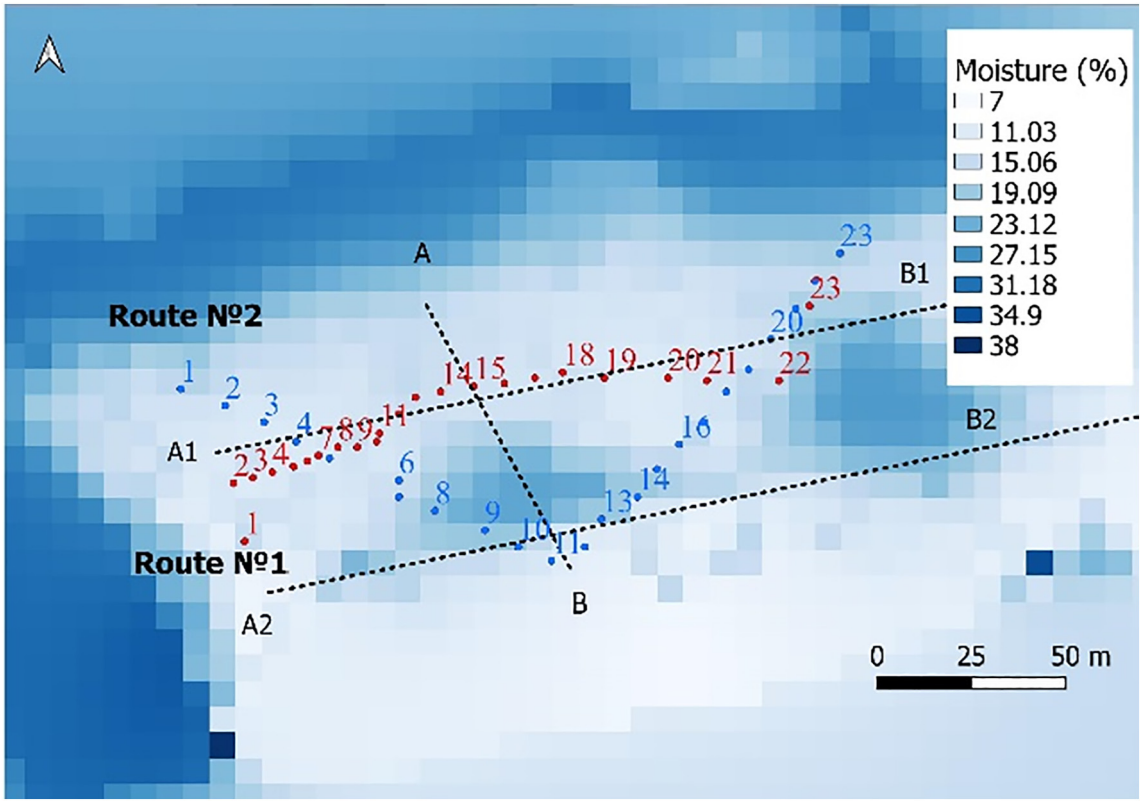

Fig. 8. Map of surface soil moisture (Θ_{ss}^{rs}) at the experimental plot based on Sentinel-1 data, created using the neural network algorithm.

moisture distribution in the SSL at an experimental plot located on agricultural land in the Volgograd region. The main feature of the proposed approach was the use of NNs to calculate the reflectivity of the soil surface, and the subsequent use of a simple algorithm to invert reflectivity into surface soil moisture using the dielectric model that considers the soil texture. Based on Sentinel-1 radar data, the proposed NN consisting of two hidden layers of *12* neurons each enabled a posteriori estimation of the spatial distribution of the surface soil moisture of the SSL at the experimental plot with a determination coefficient of *0.948* and standard deviation of *~2%*, to compare the calculated data with the soil moisture measured by the gravimetric method at the sampling sites. The developed method was tested for areas deprived of vegetation and areas with rare alfalfa vegetation.

In this study, we developed a method to perform an a posteriori estimation of surface soil moisture of SSL for values of *>14%* with an accuracy of *~2%* of the absolute values for agricultural fields, where standard deviations of soil surface elevation are *~1.5 cm*.

To use the proposed method for agricultural fields with standard deviations of soil surface elevation of *>2 cm* and surface soil moisture of SSL of *<14%*, some challenges should be addressed in future research. First, the integration of an additional parameter that reflects the variance of soil surface elevation roughness, which can be measured in the experimental plot using a UAV on the day of the Sentinel-1 passing, to improve the model. Second, further experiments are required to validate the proposed approach for cases of diverse soil texture of the SSL, as well as for the areas with agricultural crops during several vegetation stages.

Despite the above challenges, the obtained results suggest the use of the developed method to improve estimates of SSL fluctuations at the field scale for Θ_{ss} mapping and further usage of obtained data for efficient application in precision irrigation technology.

CRediT authorship contribution statement

A.M. Zeyliger: Conceptualization, Visualization, Investigation, Project administration, Methodology, Formal analysis, Writing – review & editing. **K.V. Muzalevskiy:** Conceptualization, Investigation, Software, Visualization, Formal analysis, Writing – original draft, Writing – review & editing. **E.V. Zinchenko:** Resources, Investigation, Data curation. **O.S. Ermolaeva:** Software, Validation, Methodology, Investigation, Writing – original draft.

Declaration of competing interest

The authors declare that they have no known competing financial interests or personal relationships that could have appeared to influence the work reported in this paper.

Acknowledgements

The research was performed within the framework of the Russian Foundation for Basic Research project 19-29-05261 mk “Cartographic modelling of soil moisture reserves based on complex geophysical water content measurements for digital irrigated agriculture”.

References

Andreassian, V., Bergström, S., Chahinian, N., Duan, Q., Gusev, Y.M., Littlewood, I., Mathevet, T., Michel, C., Montanari, A., Moretti, G., Moussa, R., Nasonova, O.N., Connor, K.O., Paquet, E., Perrin, C., Rousseau, A., Schaake, J., Wagener, T., Xie, Z., 2006. Large Sample Basin Experiments for Hydrological Model Parameterization: Results of the Model Parameter Experiment–MOPEX. IAHS Catalogue of the Models Used in MOPEX 2004/2005.

Baghdadi, N., Saba, E., Aubert, M., Zribi, M., Baup, F., 2011. Comparison between backscattered TerraSAR signals and simulations from the radar backscattering models IEM, Oh, and Dubois. IEEE Geosci. Remote Sens. Lett. 8, 1160–1164.

Baghdadi, N., Gherboudj, I., Zribi, M., Sahebi, M., King, C., Bonn, F., 2004. Semi-empirical calibration of the IEM backscattering model using radar images and moisture and roughness field measurements. Int. J. Remote Sens. 25, 3593–3623. https://doi.org/10.1080/01431160310001654392.

Brocca, L., Crow, W.T., Ciabatta, L., Massari, C., De Rosnay, P., Enenkel, M., Hahn, S., Amarnath, G., Camici, S., Tarpanelli, A., Wagner, W., 2017. A review of the applications of ASCAT soil moisture products. IEEE J. Sel. Top. Appl. Earth Obs. Remote Sens. https://doi.org/10.1109/JSTARS.2017.2651140.

Chen, J.M., Chen, X., Ju, W., Geng, X., 2005. Distributed hydrological model for mapping evapotranspiration using remote sensing inputs. J. Hydrol. 305, 15–39. https://doi.org/10.1016/j.jhydrol.2004.08.029.

Copernicus Open Access Hub [WWW Document], n.d. URL https://scihub.copernicus.eu/ (accessed 5.5.20).

Cloude, S., 2007. The dual polarisation entropy/alpha decomposition: a PALSAR case study. Proc. 3rd Intern. Workshop on Science and Applications of SAR Polarimetry and Polarimetric Interferometry (POLinSAR 2007), Frascati, Italy, pp. 22–26 Jan. 1–6.

Davidson, M.W.J., Le Toan, T., Mattia, F., Satalino, G., Manninen, T., Borgeaud, M., 2000. On the characterization of agricultural soil roughness for radar remote sensing studies. IEEE Trans. Geosci. Remote Sens. 38 (2), 630–640.

Dobson, M.C., Ulaby, F.T., Hallikainen, M.T., El-Rayes, M.A., 1985. Microwave dielectric behavior of wet soil-part II: dielectric mixing models. IEEE Trans. Geosci. Remote Sens. GE-23, 35–46. https://doi.org/10.1109/TGRS.1985.289498.

Dukes, M.D., Scholberg, J.M., 2004. Soil moisture controlled subsurface drip irrigation on sandy soils. Appl. Eng. Agric. 1, 89–101.

El Hajj, M., et al., 2016. Soil moisture retrieval over irrigated grassland using X-band SAR data. Remote Sens. Environ. 176, 202–218.

El Hajj, M., Baghdadi, N., Zribi, M., Bazzi, H., 2017. Synergic use of Sentinel-1 and Sentinel-2 images for operational soil moisture mapping at high spatial resolution over agricultural areas. Remote Sens. 9, 1292. https://doi.org/10.3390/rs9121292.

Entekhabi, D., Yueh, S., O'Neill, P., Kellogg, K., 2014. SMAP Handbook Soil Moisture Active Passive Mapping Soil Moisture and Freeze/Thaw From Space Pasadena.

Evans, R.G., Han, S., Kroeger, M.W., Schneider, S.M., 2015. In: Robert, P.C., Rust, R.H., Larson, W.E. (Eds.), Precision Center Pivot Irrigation for Efficient Use of Water and Nitrogen. American Society of Agronomy, Crop Science Society of America, Soil Science Society of America, pp. 75–84.

Evett, S.R., Parkin, G.W., 2005. Advances in soil water content sensing: the continuing maturation of technology and theory. Vadose Zo. J. 4, 986–991. https://doi.org/10.2136/vzj2005.0099.

Gao, H., Zhang, W., Chen, H., 2018. An improved algorithm for discriminating soil freezing and thawing using AMSR-E and AMSR2 soil moisture products. Remote Sens. 10, 1697. https://doi.org/10.3390/rs10111697.

Gowda, P.H., Chavez, J.L., Colaizzi, P.D., Evett, S.R., Howell, T.A., Tolk, J.A., 2008. ET mapping for agricultural water management: present status and challenges. Irrig. Sci. https://doi.org/10.1007/s00271-007-0088-6.

Hachani, A., Ouessar, M., Paloscia, S., Santi, E., Pettinato, S., 2019. Soil moisture retrieval from Sentinel-1 acquisitions in an arid environment in Tunisia: application of artificial neural networks techniques. Int. J. Remote Sens. 40, 9159–9180. https://doi.org/10.1080/01431161.2019.1629503.

Hallikainen, M.T., Ulabz, F.T., Dobson, M.C., El-Rayes, M.A., Wu, L.K., 1985. Microwave dielectric behavior of wet soil-part I: empirical models and experimental observations. IEEE Trans. Geosci. Remote Sens. GE-23, 25–34. https://doi.org/10.1109/TGRS.1985.289497.

IUSS Working Group WRB, 2015. World Reference Base for Soil Resources 2014, Update 2015. International Soil Classification System for Naming Soils and Creating Legends for Soil Maps. World Soil Resources Reports No. 106. FAO, Rome 192 p.

Khitrov, N.B., Omel'chenko, N.P., Nikitina, N.S., Utkaeva, V.F., Zeiliger, A.M., 2009. Preferential water flows in an ordinary Chernozem of the Azov Plain. Eurasian Eurasian Soil Sci. 42, 757–768.

Mialon, A., Richaume, P., Leroux, D., Bircher, S., Al Bitar, A., Pellarin, T., Wigneron, J.P., Kerr, Y.H., 2015. Comparison of Dobson and Mironov dielectric models in the SMOS soil moisture retrieval algorithm. IEEE Trans. Geosci. Remote Sens. 53, 3084–3094.

Mironov, V.L., Kosolapova, L.G., Fomin, S.V., 2009. Physically and mineralogically based spectroscopic dielectric model for moist soils. IEEE Trans. Geosci. Remote Sens. 47, 2059–2070.

Mirsoleimani, H.R., Sahebi, M.R., Baghdadi, N., El Hajj, M., 2019. Bare soil surface moisture retrieval from Sentinel-1 SAR data based on the calibrated IEM and Dubois models using neural networks. Sensors 19, 3209. https://doi.org/10.3390/s19143209.

Moehrlen, C., 1999. Literature review of current used SVAT models. Internal Report 04-99.

Muzylev, E.L., Startseva, Z.P., Uspensky, A.B., Volkova, E.V., Vasilenko, E.V., Kukharsky, A.V., Zeyliger, A.M., O.S., E., 2017. Using remote sensing data to model water and heat regimes of rural territories. Sovrem. Probl. distantsionnogo Zo. Zemli iz kosmosa 14, 19–47.

Oh, Y., Sarabandi, K., Ulaby, F.T., 1992. An empirical model and an inversion technique for radar scattering from bare soil surfaces. IEEE Trans. Geosci. Remote Sens. 30, 370–381. https://doi.org/10.1109/36.134086.

Overgaard, J., Rosbjerg, D., Butts, M.B., 2006. Land-surface modelling in hydrological perspective - a review. Biogeosciences https://doi.org/10.5194/bg-3-229-2006.

Paloscia, S., et al., 2013. Soil moisture mapping using Sentinel-1 images: algorithm and preliminary validation. Remote Sens. Environ. 234–248.

Paloscia, S., Pampaloni, P., Pettinato, S., Santi, E., 2008. A comparison of algorithms for retrieving soil moisture from ENVIS AT/AS AR images. IEEE Trans. Geosci. Remote Sens., 3274–3284 https://doi.org/10.1109/TGRS.2008.920370.

Pitman, A.J., 2003. The evolution of, and revolution in, land surface schemes designed for climate models. Int. J. Climatol. 23, 479–510. https://doi.org/10.1002/joc.893.

Robinson, D.A., Campbell, C.S., Hopmans, J.W., Hornbuckle, B.K., Jones, S.B., Knight, R., Ogden, F., Selker, J., Wendroth, O., 2008. Soil moisture measurement for ecological and hydrological watershed-scale observatories: a review. Vadose Zo. J. 7, 358–389. https://doi.org/10.2136/vzj2007.0143.

Startseva, Z., Muzylev, E., Volkova, E., Uspensky, A., Uspensky, S., 2014. Water and heat regimes modelling for a vast territory using remote-sensing data: International Journal of Remote Sensing: Vol 35, No 15. Int. J. Remote Sens. 35, 5775–5799.

Sui, R., Baggard, J., 2015. Wireless sensor network for monitoring soil moisture and weather conditions. Appl. Eng. Agric. 31, 193–200. https://doi.org/10.13031/aea.31.10694.

Thoma, D.P., Moran, M.S., Bryant, R., Rahman, M., Holifield-Collins, C.D., Skirvin, S., Sano, E.E., Slocum, K., 2006. Comparison of four models to determine surface soil moisture from C-band radar imagery in a sparsely vegetated semiarid landscape. Water Resour. Res. 42. https://doi.org/10.1029/2004WR003905.

Ulaby, F., Long, D., 2014. Microwave Radar and Radiometric Remote Sensing, Microwave Radar and Radiometric Remote Sensing. University of Michigan Press https://doi.org/10.3998/0472119356.

Vellidis, G., Tucker, M., Perry, C., Kvien, C., Bednarz, C., 2007. A Real-time Wireless Smart Sensor Array for Scheduling Irrigation. https://doi.org/10.1016/j.compag.2007.05.009.

Wang, H., Méric, S., Allain, S., Pottier, E., 2014. Adaptation of Oh model for soil parameters retrieval using multi-angular RADARSAT-2 datasets. J. Surv. Mapp. Eng. 2 (4), 65–74.

Wigneron, J.P., Jackson, T.J., O'Neill, P., De Lannoy, G., de Rosnay, P., Walker, J.P., Ferrazzoli, P., Mironov, V., Bircher, S., Grant, J.P., Kurum, M., Schwank, M., Munoz-Sabater, J., Das, N., Royer, A., Al-Yaari, A., Al Bitar, A., Fernandez-Moran, R., Lawrence, H., Mialon, A., Parrens, M., Richaume, P., Delwart, S., Kerr, Y., 2017. Modelling the passive microwave signature from land surfaces: a review of recent results and application to the L-band SMOS & SMAP soil moisture retrieval algorithms. Remote Sens. Environ. https://doi.org/10.1016/j.rse.2017.01.024.

Zatinatskii, S.V., Zeiliguer, A.M., Guber, A.K., Khitrov, N.B., Nikitina, N.S., Utkaeva, V.F., 2007. Preferential water flows in meadow-chernozemic soil of The Saratov Transvolga Region. Eurasian Soil Sci. 40, 532–543.

Zeng, J., Chen, K.S., Bi, H., Chen, Q., 2016. A preliminary evaluation of the SMAP radiometer soil moisture product over United States and Europe using ground-based measurements. IEEE Trans. Geosci. Remote Sens. 54, 4929–4940. https://doi.org/10.1109/TGRS.2016.2553085.

Zeyliger, A.M., Ermolaeva, O.S., Muzylev, E.L., Startseva, Z.P., Sukharev, Y.I., 2019. Computer analysis of water stress regimes of an irrigated agrocoenosis using the SWAP model and ground and space monitoring data. Sovrem.Probl. Distantsionnogo Zo. Zemli iz Kosmosa 16, 33–43. https://doi.org/10.21046/2070-7401-2019-16-3-33-43.

Zhang, L., Meng, Q., Hu, D., Zhang, Y., Yao, S., Chen, X., 2020. Comparison of different soil dielectric models for microwave soil moisture retrievals. Int. J. Remote Sens. 41, 3054–3069. https://doi.org/10.1080/01431161.2019.1698077.